Design, additive manufacturing and component testing of pneumatic rotary vane actuators for lightweight robots

Gabriel Dämmer
Advanced Development Control and Robotics, Festo SE & Co. KG, Esslingen, Germany and
Institute of Polymer Product Engineering, Johannes Kepler Universitat Linz, Linz, Austria
Hartmut Bauer and Rüdiger Neumann
Advanced Development Control and Robotics, Festo SE Co. KG, Esslingen, Germany, and
Zoltan Major
Institute of Polymer Product Engineering, Johannes Kepler University Linz, Linz, Austria

Abstract

Purpose – This study aims to investigate the suitability of a multi-step prototyping strategy for producing pneumatic rotary vane actuators (RVAs) for the development of lightweight robots and actuation systems.

Design/methodology/approach – RVAs typically have cast aluminum housings and injection-molded seals that consist of hard thermoplastic cores and soft elastomeric overmolds. Using a combination of additive manufacturing (AM), computer numerical control (CNC) machining and elastomer molding, a conventionally manufactured standard RVA was replicated. The standard housing design was modified, and polymeric replicas were obtained by selective laser sintering (SLS) or PolyJet (PJ) printing and subsequent CNC milling. Using laser-sintered molds, actuator seals were replicated by overmolding laser-sintered polyamide cores with silicone (SIL) and polyurethane (PU) elastomers. The replica RVAs were subjected to a series of leakage, friction and durability experiments.

Findings – The AM-based prototyping strategy described is suitable for producing functional and reliable RVAs for research and product development. In a representative durability experiment, the RVAs in this study endured between 40,000 and 1,000,000 load cycles. Frictional torques were around 0.5 Nm, which is 10% of the theoretical torque at 6 bar and comparable to that of the standard RVA. Models and parameters are provided for describing the velocity-dependent frictional torque. Leakage experiments at 10,000 load cycles and 6 bar differential pressure showed that PJ housings exhibit lower leakage values (6.8 L/min) than laser-sintered housings (15.2 L/min), and PU seals exhibit lower values (8.0 l/min) than SIL seals (14.0 L/min). Combining PU seals with PJ housings led to an initial leakage of 0.4 L/min, which increased to only 1.2 L/min after 10,000 load cycles. Overall, the PU material used was more difficult to process but also more abrasion- and tear-resistant than the SIL elastomer.

Research limitations/implications – More work is needed to understand individual cause–effect relationships between specific design features and system behavior.

Originality/value – To date, pneumatic RVAs have been manufactured by large-scale production technologies. The absence of suitable prototyping strategies has limited the available range to fixed sizes and has thus complicated the use of RVAs in research and product development. This paper proves that functional pneumatic RVAs can be produced by using more accessible manufacturing technologies and provides the tools for prototyping of application-specific RVAs.

Keywords Actuators, Functional testing, Moulding, Polymers, Robotics, Additive manufacturing

Paper type Research paper

1. Introduction

In recent years, researchers and engineers have worked continuously toward compactness, cost-efficiency and the ability of lightweight robots to perform dexterous tasks, such as those required in human–robot interaction (Haddadin, 2013; ISO/TS 15066:2017–04, 2017; Zinn *et al.*, 2004). In this context, double-acting pneumatic actuators have been discussed because, unlike electromechanical approaches (Grebenstein *et al.*, 2011), they inherently offer adjustable compliance (Baiden and Ivlev, 2014; Vanderborght *et al.*, 2013; Veale and Xie, 2016) without an increase in mechanical complexity. Researchers have used pneumatic bellows

The current issue and full text archive of this journal is available on Emerald Insight at: **https://www.emerald.com/insight/1355-2546.htm**

Rapid Prototyping Journal
28/11 (2022) 20–32
Emerald Publishing Limited [ISSN 1355-2546]
[DOI 10.1108/RPJ-03-2021-0052]

Received 7 March 2021
Revised 6 January 2022
27 February 2022
Accepted 28 February 2022

actuators to actuate manipulators of continuum (Grzesiak *et al.*, 2011; Raisch *et al.*, 2020), articulated (Gaiser *et al.*, 2012) and mixed (Festo SE & Co. KG, 2019) kinematic types. However, use of bellows actuators typically limits the range of motion and results in angular dependency of torque. Further, ensuring structural integrity of the deformable bellows chambers is challenging if the supply pressure is set to the industry standard of 6 bar (Müller and Nau, 1998) and hundreds of thousands of load cycles must be endured. Researchers have recently overcome these drawbacks to some degree by using pneumatic rotary vane actuators (RVAs) to actuate the "BionicCobot" conceptual robotic arm (Festo SE & Co. KG, 2019). Each of the robot's seven joints has a modified standard RVA. Figure 1 presents detailed views of a standard RVA DRVS-25–270 (Festo SE & Co. KG, 2020), that resembles those used in the "BionicCobot". The RVA consists of a top housing, a bottom housing (not shown), a rotary vane that is attached to a drive shaft and a chamber seal that is fixed to the housings. Rotary vane and chamber seal consist of hard thermoplastic cores and soft elastomeric overmolds. Ball bearings (not shown) in the housing enable low-friction rotation of the shaft.

The housings form a closed volume that is divided by the rotary vane and the chamber seal into two distinct pressure chambers [Figure 1(b)]. When pressure is applied to the chambers, the rotary vane translates the pressure forces acting on its sides into torque about its center axis. Thus, the resulting torque is a function of the pressure differential p_1–p_2 and of the effective area A and radius r_{eff} of the rotary vane. The corresponding equation of motion is given by:

$$\mathcal{J}\,\ddot{\varphi} = \sum_k T_k = (p_1 - p_2)\cdot A \cdot r_{eff} - T_F(\varphi) - T_G - T_L, \quad (1)$$

where $\mathcal{J}$ and $\ddot{\varphi}$ are the inertia and the angular acceleration of the rotating parts, respectively. Frictional torques T_F result from the contact between chamber seal and vane, and between vane and the housing's lateral and end faces, as indicated by Labels 2, 3 and 4 in Figure 1(b), respectively. Further, external loads T_L and gravitational loads T_G are considered. Standard RVAs have been developed for industrial automation purposes, and their use in future lightweight robots would require considerable design modifications to increase power-to-weight ratio. Today's standard RVAs are manufactured by large-scale production technologies at high tooling costs and long lead times. To evaluate optimized RVA versions, quick and cost-efficient prototyping methods, such as additive manufacturing (AM), are required. While prototyping of inflatable pneumatic actuators for soft robotics has become a popular research topic (Gorissen *et al.*, 2017; Schmitt *et al.*, 2018; Wallin *et al.*, 2018; Yap *et al.*, 2020; Zolfagharian *et al.*, 2016), prototyping, and especially AM, of RVAs remains nearly unexplored. This is unsurprising, because dimensional accuracy and surface quality are typical weak points of AM processes (MacCurdy *et al.*, 2016; Neitzert, 2015; Rebong *et al.*, 2018;) but are essential for RVAs to function properly (Remmers *et al.*, 2010). Pneumatic cylinders have been manufactured using fused filament fabrication (Krause and Bhounsule, 2018; Varga and Filakovsky, 2020). Varga and Filakovsky (2020) attempted to entirely FDM print the actuators and confirmed problems related to surface quality and dimensional accuracy. Krause and Bhounsule (2018) used a combination of printed polymeric and standard metallic parts and demonstrated that dynamic sealing between piston and cylinder can be achieved by surface postprocessing the FDM parts in combination with the use of commercial O-ring seals. As indicated in Figure 1, rotary vanes contain various seals (2, 3, 4) that cannot be replaced by simple O-rings. The RVAs' rotary vanes and chamber seals require combined manufacturing of rigid core materials and soft but resilient elastomers. However, for direct AM of complex multi-material components, only a few technologies are available. The most wide-spread commercial option is the PolyJet (PJ) process (Siegfarth *et al.*, 2020), in which objects of desired shapes are accumulated from droplets of acrylate-based photocurable ink that are deposited via piezo nozzles and cured by infrared light. Kundera and Bochnia (2014) fabricated O-ring seals using PJ technology and found that, although the seals were usable, they exhibited complex time-dependent mechanical behavior. Paydar *et al.* (2014)

Figure 1 Main components of a standard pneumatic RVA for industrial use (Festo SE & Co. KG, 2020) with machined aluminum housings and injection-molded polymer components (a). Identification of the chamber pressures p_1 and p_2, sealing points (1–4) and angular deflection φ (b)

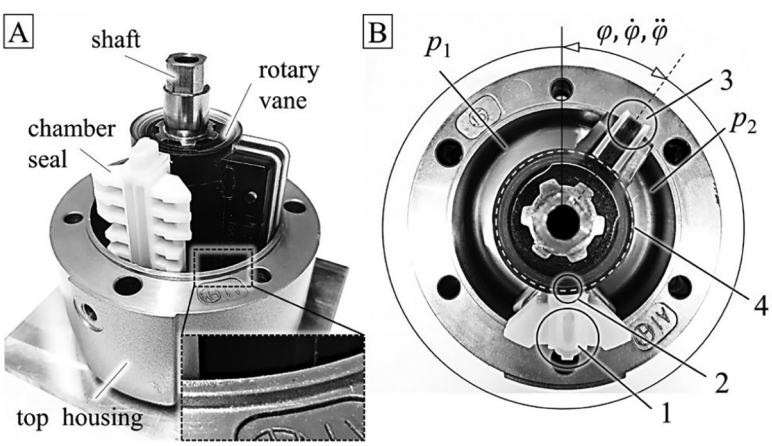

investigated multi-material PJ-printed interconnect devices for microfluidics and reported that repeated use of the gaskets reduced the applicable pressure significantly. Siegfarth *et al.* (2020) produced multi-material miniature hydraulic piston actuators with integrated elastomeric seals and investigated their leakage, friction and durability. Based on the experimental results, Siegfarth *et al.* (2020) suggested that the durability of the PJ materials used might be sufficient for short-term and single-use devices. Generally, elastomeric PJ materials undergo fatigue if subjected to repeated loadings (Dämmer *et al.*, 2019; Kaweesa and Meisel, 2018; Moore and Williams, 2015), which further complicates their use. However, weaknesses in material quality and dimensional accuracy of direct AM approaches can be overcome by introducing additional manufacturing steps. Many researchers have applied AM to produce molds (Kampker *et al.*, 2017; Udroiu and Braga, 2017) for elastomers (Florez *et al.*, 2014; Galloway *et al.*, 2013; Galloway *et al.*, 2016; Li *et al.*, 2020; Mosadegh *et al.*, 2014; Sun *et al.*, 2013). Remmers *et al.* (2010) developed RVAs with additively manufactured housings and rotary vanes. Relevant housing surfaces were machined, and the rotary vanes were equipped with molded elastomeric seals. Further, they reported leakage at higher pressures and pointed out that the most challenging part was fabrication of the elastomeric seals. Remmers *et al.* (2010) also demonstrated overmolding of the printed rotary vanes with a silicone elastomer but were not able to test the parts before publication. In summary, prototyping of pneumatic actuators, seals and fluidic devices has been the subject of numerous studies, but only Remmers *et al.* (2010) have directly addressed the AM-based prototyping of pneumatic RVAs. Consequently, it remains unclear if and how functional RVA prototypes can be produced and whether their quality would be sufficient for concept evaluation in the context of pneumatic lightweight robots. Considering that direct multi-material AM remains limited to elastomers with inferior material properties, it seems more promising to use printed molds to produce an RVA's elastomeric components. This paper presents the replication of the conventionally manufactured standard actuator shown in Figure 1 without use of mass-production technologies. Sections 2–4 describe design, manufacturing and component testing of AM-based RVAs, respectively. This work builds on the EU-funded DIMAP research project (GA 685937) and contributes to the development of an additively manufactured pneumatic lightweight robot that will be described in a future publication.

2. Design of additive manufacturing-based rotary vane actuators

2.1 Redesign of rotary vane actuator housings

This section describes the redesign of standard RVA aluminum housings for manufacturing with polymeric AM materials: top and bottom housings are aligned via a centering ring that is shown in the magnified image of Figure 1(a). Four bolts connect the top and bottom housing and are preloaded so that adequate contact pressure between centering ring and top housing is maintained during operation. The polymeric AM materials used to replicate the housings are the thermoplastic polyamide PA2200 (EOS GmbH, 2018) and the thermosetting acrylate-based photopolymer VeroWhitePlus (Stratasys Ltd, 2018). Both materials provide significantly lower stiffness and strength than the aluminum used for the standard housings. To avoid excessive deformation and structural failure of the centering ring, the housings were redesigned using finite element analysis (FEA). Figure 2(a) illustrates the meshed assembly for FEA, which consists of 30° housing sections and a bolt section. In the initial load step, a bolt force of 400 N was applied, and the resulting bolt length was fixed for the rest of the analysis. In the second load

Figure 2 The simulation-based design shown in A, B, C ensured structural integrity and air tightness

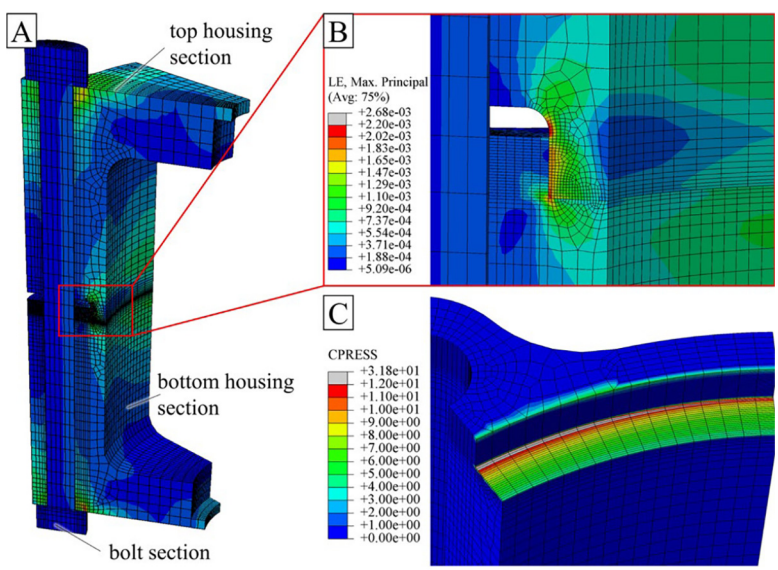

Notes: (A) Shows the simulation-based redesign of polymeric RVA housings; (B) shows the evaluation of strains; (C) shows the evaluation of contact pressures

step, a pressure of 6 bar was applied to the inner surfaces of the housing. A friction coefficient of 0.3 was defined between parts in contact. To describe the time-dependent small-strain behavior of the housing materials, a linear-elastic–linear-viscoelastic material model was chosen. To approximate the initial stiffness of the materials used, a Young's modulus of 2,500 MPa and a Poisson's ratio of 0.4 were defined. To account for time-dependency of the mechanical stiffness typical for polymers, a Prony series was formulated, which causes an exponential decrease in the Young's modulus (Bergström, 2015) to 60% of its initial value. While more detailed modeling of the polymers used exceeds the scope of this paper, further studies have been published (Salmoria *et al.*, 2012; Zhang and To, 2016).

A suitable geometry of the centering ring was determined by multiple iterations of design modification and structural analysis. We used eight M3 bolts to improve homogeneity of contact pressure between the centering ring and bottom housing. Further, we increased the thickness of the centering ring to 2.5 mm and increased the radius at the transition to 2.0 mm to reduce strains. Figure 2(c) plots the contact pressure distribution of the sealing surface at the end of the second load step. The simulated contact pressure in the relevant area was around 5 MPa, which is well above the fluid pressure of 0.6 MPa. The largest maximum principal strains occurred in the initial step at the radius of the centering ring (B) and were below 0.27%, which we consider to be uncritical. This was a promising starting point, but an approximate simulation cannot cover all effects of short- and long-term variations of loads and temperatures on the structural behavior. Functionality and durability of the redesigned polymer housings were therefore validated in component tests, as described in Section 4. Based on the FEA model, modified housings were designed in computer-aided design (CAD) software. In Figure 3, the final housing design is shown as part of the actuator assembly. In contrast to the standard RVA, the pressure sensors can be attached directly to the top housing.

Figure 3 CAD model of a pneumatic RVA with additively manufactured polymer housings, rotary vane and chamber seal

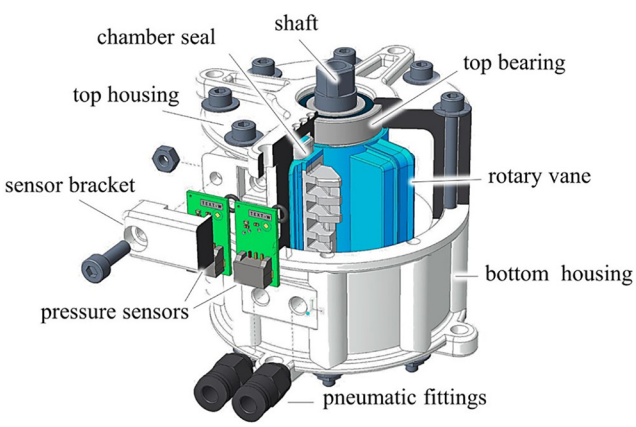

Notes: While the inner contour of the housing corresponds to the original, the screw connections and the centering ring were modified to allow the use of polymers. A connection for pressure sensors was integrated into the housing

2.2 Design of additive manufacturing molds

For manufacturing of the multi-material rotary vane and chamber seal, a multi-step prototyping sequence was developed by building on related work (Remmers *et al.*, 2010): in the sequence, rigid cores are obtained by SLS, placed in the cavity of an additively manufactured mold and then over-molded by liquid elastomer precursors. Figure 4 shows an exploded view of the mold assembly. The cavity which defines the shape of the elastomeric overmold is formed by three mold pieces (right, left and center) and the vane core. In the first assembly step, the vane core is placed in the center mold. A profiled fixation shaft is then inserted through the center mold and vane core. Using a screw and a threaded cap, the center mold is pressed against the side surfaces of the core and seals the cavity there. The left and right mold pieces are joined laterally, where exact alignment is ensured by integrated centering rings. Bolts hold together the mold pieces and fix them to a stand that facilitates curing in an upright position. A disposable sprue and risers are attached to the mold to complete the assembly. The elastomeric overmold is illustrated in blue.

3. Manufacturing of additive manufacturing-based rotary vane actuators

3.1 Manufacturing of housings

The housings of our prototypic RVAs were manufactured by PJ printing of the acrylate-based thermosetting photopolymer VeroWhitePlus (Stratasys Ltd, 2018) and SLS of a thermoplastic polyamide powder (EOS GmbH, 2018). Layer thicknesses of 0.016 and 0.1 mm were used for the PJ and SLS parts, respectively. The housings were oriented with the main diameter being parallel to the printing platform. As described by Remmers *et al.* (2010) and confirmed by our own experiments, direct printing of the housings without an additional machining step resulted in excessive leakage. For this reason, all friction surfaces and the centering ring of our RVAs were printed 1.0 mm over size and then computer numerical control (CNC) milled to nominal dimensions, as shown in Figure 5(a). All milling operations were performed using a torus mill with a diameter of 4 mm and an edge radius of

Figure 4 Mold assembly used for manufacturing of rotary vanes

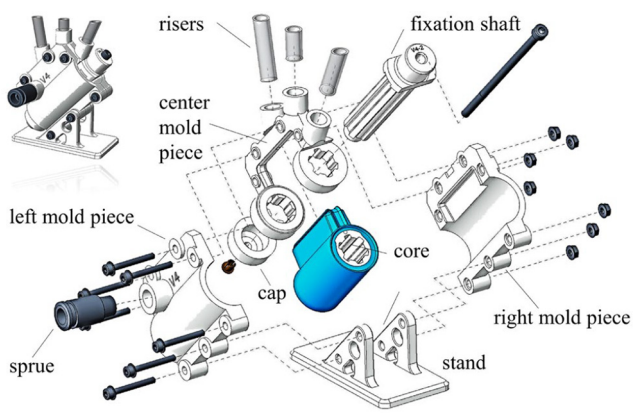

Note: A thermoplastic vane core is placed in the cavity of an additively manufactured mold and overmolded with elastomeric material (blue)

Figure 5 CNC milling operations (a) and clamping (b) of polymer housings for pneumatic RVAs

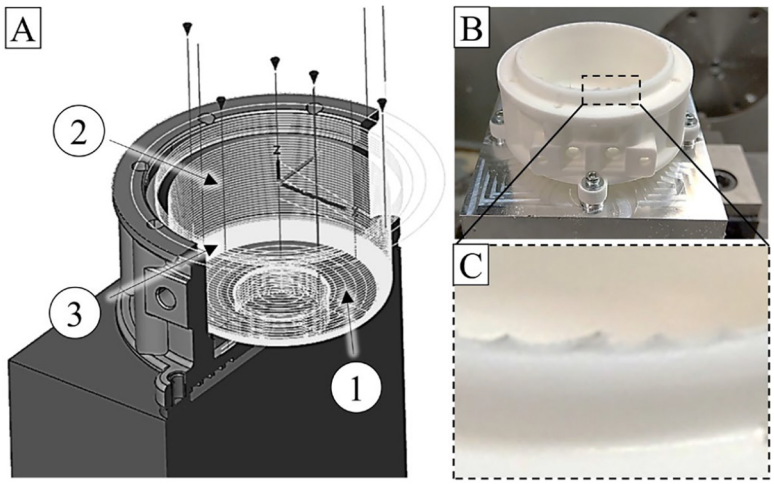

Note: The quality of milled edges is better on the thermoset PJ housings than on the thermoplastic SLS housings (c)

0.3 mm. In the first step, plane surfaces were milled applying a pattern of concentric circles (1) with radial steps of 2 mm. The cylindrical surface (2) and the radius (3) were then machined by circular milling at spindle speeds of 6,764 and 8,000 1/min and feed rates of 757 and 1500 mm/min, respectively. Helical paths were followed with pitches of 0.6 mm/rotation for the cylindrical surface and 0.07 mm/rotation for the radius. As shown in Figure 5(b), the housings were attached to four screw points to allow machining in one clamping with minimal distortion. We found that the machined edges of the thermoplastic SLS housings were slightly frayed, as shown in Figure 5(c), which was not the case with the thermoset PJ parts.

3.2 Manufacturing of elastomeric seals

We used a silicone elastomer (SIL) of Shore 50 A (Smooth-On, Inc., 2022a) and a polyurethane (PU) elastomer of Shore 80 A (Smooth-On, Inc., 2022b) hardness to mold the soft components of the RVAs' rotary vanes and chamber seals. In Table 1, characteristic properties of both materials are compared. Both elastomers were processed at ambient temperature and polymerized by a polyaddition reaction without by-products and no relevant shrinkage occurred. Liquid urethanes absorb atmospheric moisture, which limits their shelf-life and may cause the formation of CO_2 bubbles in the cured PU parts. Furthermore, pot life of the mixed PU precursors is only 25 min, which limited the number of parts per batch. Safety procedures had to be followed, because a PU precursor contains potentially hazardous toluene diisocyanate (Smooth-On, Inc., 2021). Processing of the SIL material used was significantly simpler because of the absence of hazardous components and a pot life of 45 min. Note that we observed cure inhibition when SIL was processed in combination with PJ molds and without adequate preparation. In terms of mechanical properties, the PU is clearly superior, with an elongation at break of 750%, which is more than twice that of SIL (320%). Moreover, the tear strength of the silicon elastomer used is significantly smaller (155 ppi – pounds per linear inch) (Smooth-On, Inc., 2022a) than that of the PU (200 ppi) (Smooth-On, Inc., 2022b). Note that the tear strength of SIL given in the datasheet was determined by using the round-notched "Die B" specimens rather than the rectangular-notched "Die C" specimens that were used for the PU.

Table 1 Comparison of elastomeric materials for the manufacturing of functional dynamic seals

Group of elastomers	Silicone (SIL)	Polyurethane (PU)
Product name	Smooth-Sil 950	PMC-780 Dry
Polymerization issues	Cure inhibition	Side reaction, CO_2
Mixed viscosity (cps)	35,000	2,000
Pot life (min)	45	25
Cure time (h)	18	48
Hazardous components	–	Toluene diisocyanate
Shore A hardness	50	80
100% modulus (MPa)	1.9	2.8
Elongation at break (%)	320	750
Tear strength (ppi)	155 (Die B)	200 (Die C)

Notes: Values were taken from material data sheets (Smooth-On, Inc., 2022a, 2022b) and material safety datasheets (Smooth-On, Inc., 2020, 2021)

Before assembly, molds were cleaned carefully and coated with sealing and release agents to prevent adhesion (Smooth-On, Inc., 2022b) and to facilitate demolding of the delicate elastomeric structures. Sealing agent was applied before every fifth batch and release agent before every batch. When molding SIL parts using polyamide (SLS) molds, this procedure is not obligatory, but sealing the surfaces leads to slightly improved surface quality and facilitates demolding. The SLS molds were assembled as shown in Figure 4. Elastomer precursors were stirred in their original containers, poured into polymer cups and mixed in accordance with the datasheets (Smooth-On, Inc., 2022a, 2022b). Wooden and stainless-steel stirring rods were used for the SIL and the PU materials, respectively. Containers with mixed precursors were then degassed in a

vacuum chamber at 0.1 bar absolute pressure for several minutes. In the SIL material, air bubbles can be removed completely by this procedure. In the PU material, however, gas bubbles do not originate exclusively from mechanical processing, but also emerge as a result of a chemical side reaction. We observed that, if PU material from reopened containers was used, vacuuming to a bubble-free state was not possible within pot life of the material. In the subsequent processing step, the material was poured into a syringe and pressed through the sprue into the cavity of the mold and risers. The sprue was closed with a plug, and molds were stored in an upright position. While SIL parts were cured at ambient pressure, PU molds were placed into a pressure chamber that was pressurized with 6 bar (relative pressure) to collapse existing gas bubbles and avoid formation of new ones.

3.3 Actuator assembly

Figure 6(a) shows one of our AM-based RVAs in half-assembled state. The actuator comprises SLS housings and blue SIL parts that were manufactured following the procedures described in Sections 3 A and B, respectively. Figure 6(b) presents the subassemblies and individual parts required to assemble the complete RVA. The mass of each subassembly is given for different manufacturing variants, including the standard (STD) assembly. Our AM-based RVAs weigh only 202.9–225.3 g, which is a significant step toward the intended use in lightweight robots compared to the 473.1 g of the standard RVA. This mass reduction can be attributed mainly to replacing the standard 317.6 g aluminum housings with polymeric housings that weigh only 74.3 g (SLS) and 94.4 g (PJ). Shortening and drilling through the standard steel shaft reduced its mass from 86.1 to 47.8 g. Use of an aluminum (Al) shaft would reduce the mass by a further 31.3 g. Structural optimization of the housings and use of smaller diameter screws hold further potential for mass reduction.

4. Component testing of additive manufacturing-based rotary vane actuators

4.1 Overview of components

For component testing, four RVA variants were created that differed in the materials used. As each variant was manufactured twice, eight RVAs were available in total. In Table 2, their nomenclature is explained. Before assembly, friction surfaces were lubricated with a silicone-based grease (Unisilikon L641, Klüber Lubrication SE & Co. KG). All housing bolts were tightened to 0.2 Nm in a star pattern.

For the RVAs described in this paper, we used molds and cores of the same thermoplastic material as for the SLS housings (EOS GmbH, 2018). However, functional molds and cores can also be manufactured by PJ printing of the housing material (Stratasys Ltd, 2018). We found that PJ cores and molds break easily because of the brittleness of the material. PJ molds can also cause cure inhibition of the SIL material.

4.2 Experimental setup and testing procedure

4.2.1 Experimental setup

To prove the overall functionality and evaluate the leakage, friction and durability properties of the RVAs presented, a suitable hardware setup and an experimental procedure were developed. The experimental setup is shown in Figure 7 (right) and consisted of two Festo MPYE-5-M5-LF proportional valves, a SFAB-10U-HQ6 or SFAB-200U-HQ6 flow sensor, two SPTE-P10-R-Q4 pressure sensors, the RVA and a Heidenhain ECI 11118 rotary encoder (4). A dSPACE (dSPACE GmbH) prototyping computer (not shown) with a DS1005 processor card was used to control the valves and capture the sensor data. The processor card was programmed via Matlab/Simulink (The MathWorks, Inc.). For investigating frictional properties and mechanical durability, arbitrary reference trajectories of the target pressures could be defined in Simulink and sent via the real-time interface.

Figure 6 AM-based RVA with SLS housings and SIL seals in half-assembled (a) and fully disassembled (b) states

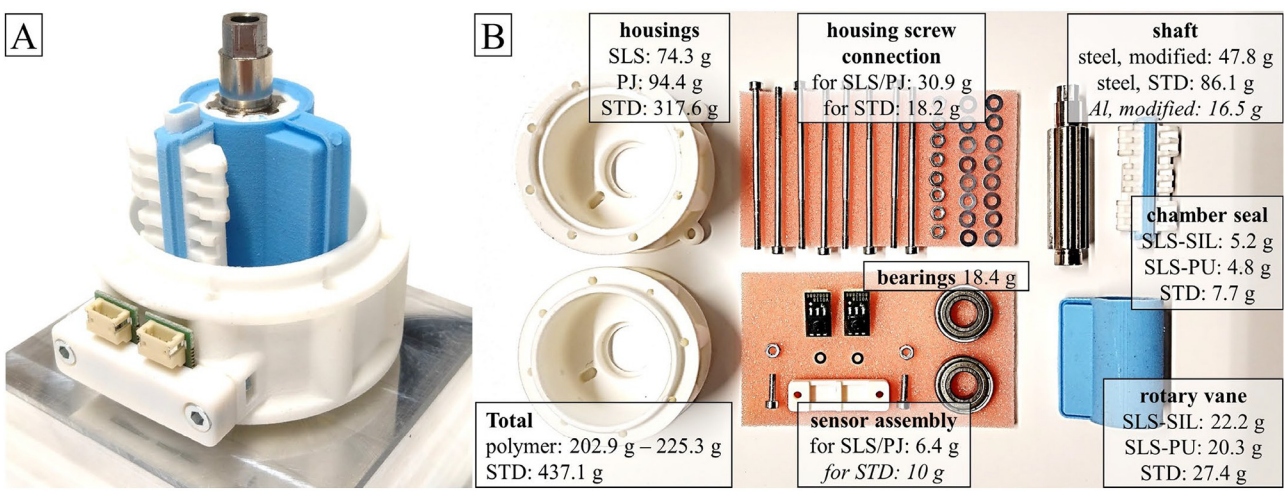

Notes: The AM-based replicas presented have a significantly reduced mass compared to the standard (STD) RVA. Mass reduction can be attributed mainly to the housing design and materials

Table 2 Manufacturing variants and nomenclature of AM-based RVAs investigated in this paper

Seals		Housings	
Hard component	**Soft component**	**SLS, polyamide**	**PJ, acrylate-based thermoset**
SLS, polyamide	molding, silicone	SLS-SIL-1 SLS-SIL-2	PJ-SIL-1 PJ-SIL-2
SLS, polyamide	molding, polyurethane	SLS-PU-1 SLS-PU-2	PJ-PU-1 PJ-PU-2

Note: "SLS-SIL-1", for example, identifies one of two RVAs with SLS housings and SIL seals

Figure 7 Overall testing procedure and hardware setup for the quality assessment of AM-based RVAs

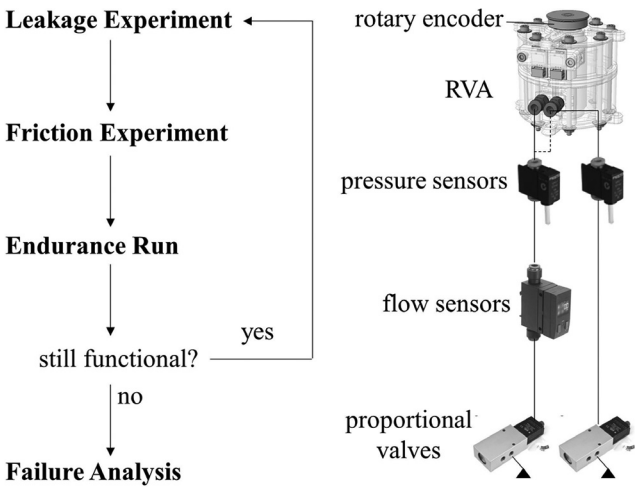

4.2.2 Overall testing procedure

Using the experimental setup described above, RVAs were subjected to a series of experiments, as shown in Figure 7 (left). First, each RVA was inspected for leakage flows between the pressure chambers and for airflow to the environment. Frictional torques were then measured at two different zero positions of the rotary vane. The RVA then underwent an endurance run of a defined number of load cycles while being position-controlled using a sinusoidal target profile. If the RVA remained functional after the endurance run, the sequence of experiments was repeated. Otherwise, the RVA was inspected for signs of wear and structural damage.

4.3 Leakage of additive manufacturing-based rotary vane actuators

4.3.1 Leakage experiment

To evaluate the airtightness of the RVAs, leakage experiments were performed as part of the overall testing procedure shown in Figure 7. For functional drives, leakage to the environment was found to be below the measuring accuracy of 0.1 l/min and therefore not investigated further. Leakage – hereafter defined as the volume flow between the pressure chambers – was measured in both directions: p_1 = 6 bar and p_2 = 0 bar; p_1 = 0 bar and p_2 = 6 bar. Between leakage measurements, the RVAs were rotated in 45° steps, starting from a vane position of 135° and reaching an angle of −135°. At each angular position, the rotary vane was mechanically blocked and the flow rates to the pressure chambers were captured. The flow rates turned out to increase within the first few seconds of pressurization, and thus the values were measured as soon as the flow rate started to fluctuate.

4.3.2 Results of leakage experiments

In Figure 8, leakages of the different manufacturing variants are compared between 0 and 100,000 load cycles. Linear regressions are used here for the sake of clarity and measurements of both actuator chambers at all seven angular positions are considered. The leakages measured ranged from lower values close to 0.0 L/min for PJ-PU RVAs to more than 50.1 L/min one of the PJ-SIL RVAs.

Clear differences can be observed for the initial leakage, the increase in leakage and the total number of load cycles performed. For detailed discussion, leakage values at 0 and 10,000 load cycles are compared in Table 3. If unavailable, values at 10,000 load cycles were interpolated linearly between neighboring values. Additionally, averaged values for each manufacturing variant are given. Generally, leakage increased during the first 10,000 load cycles. In our experiments, RVAs with PJ housings showed less leakage than those with SLS housings, and RVAs with PU seals leaked less than those with SIL seals. This relation holds at 0 and at 10,000 load cycles.

Figure 8 Leakage in different manufacturing versions of AM-based RVAs

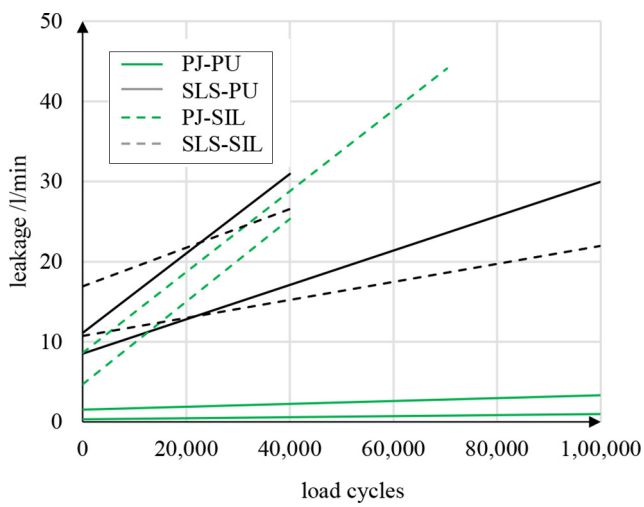

Note: Curves are linear regressions of the measured values

Table 3 Leakage of AM-based RVAs in L/min at 0 and 10,000 load cycles

	SLS housings		PJ housings		Average	
Load cycles	**0**	**10,000**	**0**	**10,000**	**0**	**10,000**
PU seals	6.4	14.9	0.4	1.2	3.4	8.0
SIL seals	13.9	15.6	6.8	12.4	10.4	14.0
Average	10.1	15.2	3.6	6.8	Leakage in L/min	

Note: The lowest leakage values were achieved by combining PJ housings with PU seals

Thus, the lowest leakages were obtained by a combination of PJ housings and PU seals with 0.4 L/min at 0 load cycles and 1.2 L/min at 10,000 load cycles. Combining SLS housings with SIL seals resulted in average leakage values of 13.9 and 15.6 L/min at 0 and 10,000 load cycles, respectively.

Remarkably, the combination of PJ housings and PU seals did not only correlate with the lowest leakage flows, but also reached the highest numbers of load cycles. This is shown in Figure 9, where the course of leakage flow over the number of load cycles performed is plotted for both RVAs of this combination. Leakage values for Chamber 1 and Chamber 2 are shown separately in addition to average values. Generally, PJ-PU-2 exhibited lower leakage values than PJ-PU-1. At 0 load cycles, the measured leakage was 0.2 L/min for PJ-PU-2 and 0.6 L/min for PJ-PU-1. Throughout the experiment, these values increased to 3.7 L/min for PJ-PU-2 and 12.8 L/min for PJ-PU-1. Both sets of housings were of similar quality, and seals were molded in the same batch. The lower leakage of PJ-PU-2 is most likely because of a slightly thicker chamber seal that was obtained from a different mold.

4.3.3 Discussion of leakage experiments

For comparison, we tested a standard actuator at up to 100,000 load cycles, but leakage values remained below the measuring accuracy of 0.1 L/min. Our AM-based RVAs clearly exceeded this value. However, small and relatively consistent leakage, such as that observed for the PJ-PU RVAs, seems unproblematic for the intended use in robotics and can easily be compensated for by feedback control. The measured leakage values reflect a combination of several factors, such as surface roughness and contact pressure (Müller and Nau, 1998). However, because all housings were CNC machined and geometrically measured, we consider the influences of geometric deviations and housing surfaces to be negligible. The difference in initial leakage between SLS housings (10.1 L/min) and PJ housings (3.6 L/min) seems to be because of another effect. Presumably, the relatively low edge quality of SLS housings, as shown in Figure 5(c), causes increased leakage. Further, we assume that lower contact pressure and excessive wear of the SIL seals explain the increased leakage values.

Figure 9 Comparison of leakage flows in AM-based RVAs with PU seals and PJ housings

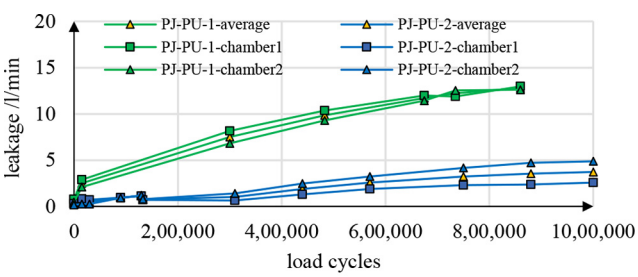

Note: Leakage flows of the PJ-PU-1 and PJ-PU-2 actuators are plotted in green and blue, respectively

4.4 Friction of additive manufacturing-based rotary vane actuators

4.4.1 Friction experiment

For friction testing, RVAs were position-controlled using a sinusoidal target profile according to

$$\varphi(t) = \varphi_{\text{amp}} \cdot \sin(\omega \cdot t) + \varphi_{\text{off}}. \tag{2}$$

An angular frequency of $\omega = 2\pi$/s and an amplitude φ_{amp} of 55° were defined. The experiment was repeated with the offset angles $\varphi_{\text{off}} = 0°$ and $\varphi_{\text{off}} = 55°$, and a mean pressure of $p_{\text{mean}} = (p_1 + p_2)/2 = 4$ bar was set. Each experiment was run for 25 s, and pressure and position signals were captured at a sampling frequency of 1,000 Hz. In Figure 10, the target and actual values of angular position, velocity and acceleration are shown together with the actual chamber pressures p_1 and p_2. Angular velocity and acceleration are the first and second time-derivatives of the position signal, respectively. Data were obtained by testing the PJ-PU-2 drive at 7,500 load cycles.

Frictional torque were calculated by solving the equilibrium of torques [equation (1)] for the frictional torque:

$$T_{\text{F}}(\varphi) = (p_1 - p_2) \cdot A \cdot r_{\text{eff}} - \mathcal{J}\ddot{\varphi} - T_{\text{G}} - T_{\text{L}}. \tag{3}$$

A similar method is typically used to identify friction parameters of pneumatic cylinders, as shown by Helduser and Muth (1996). In the setup used, gravitational torques T_G were minor, and no external loads T_{L} were applied. Because of the sinusoidal position profile [equation (2)], and as shown in Figure 10, angular velocity $\dot{\varphi}$ and acceleration $\ddot{\varphi}$ undergo constant change. Assigning values for $T_{\text{F}}(\ddot{\varphi})$ to corresponding angular velocities $\dot{\varphi}(t)$ for the experimental time period yields the friction curve $T_F(\dot{\varphi})$, a typical example of which is given in Figure 11. A clear visual distinction can be made between values of the acceleration and deceleration phases. Similar behavior was also described in (Belforte *et al.*, 2013; Hildebrandt *et al.*, 2009) and attributed to the pressure control and pressure-dependent contact force of the rotary vanes' lip seals. Generally, frictional torque was strictly monotonically increasing with angular velocity. The typical friction overshoot (Helduser and Muth, 1996; Schlüter and Perondi, 2018) was not observed in our experiments, which is because of the use of a silicone-based lubrication grease.

We modeled this frictional behavior by means of a hyperbolic tangent expression:

$$T_{\text{F}}(\dot{\varphi}) = a \cdot \tanh(b \cdot \dot{\varphi}) + c \cdot \dot{\varphi} \tag{4}$$

where a denotes the height of the transition (which relates to sticking friction) and c defines the gradient at high velocities (which relates to viscous friction), as plotted in Figure 11. Parameter b describes the gradient at low velocities and was set

Figure 10 Target and actual values of angular position, speed and acceleration and of chamber pressures during the friction experiment conducted with AM-based RVAs

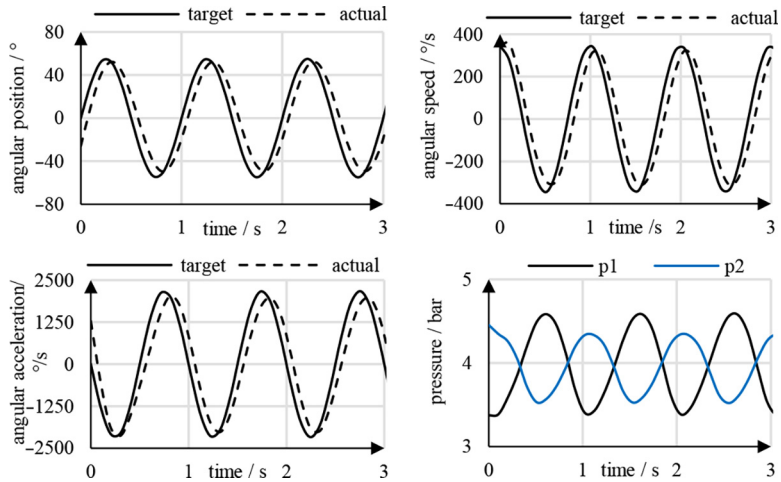

Figure 11 Measurement (black dots) and approximation (blue curve) of velocity-dependent friction in RVAs with example data

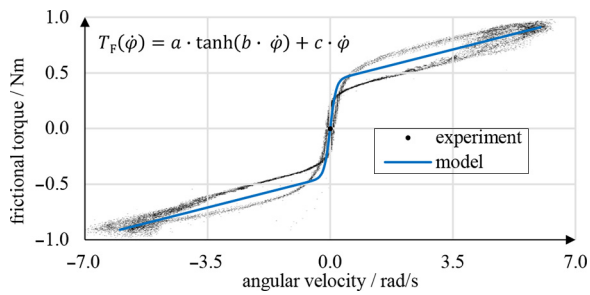

to a value of 100. For each friction measurement performed, we determined a friction curve by fitting equation (4) to experimental data, using a non-linear least-squares method implemented in Matlab (The MathWorks, Inc.).

4.4.2 Results of friction experiments

Figure 12 plots modeled friction curves $T_F(\varphi)$ of the four manufacturing variants. Each curve is an average of data recorded after 5,000–40,000 load cycles, considering both offset angles (0° and 55°). Measurements at smaller numbers of load cycles were not considered to exclude running-in behavior. The friction model equation and the parameter values are also given in Figure 12.

Between 1 and 4 rad/s, frictional torques were between 0.3 and 0.7 Nm, which corresponds to 6% and 14% of the theoretical maximum torque of 5 Nm at 6 bar. Clear differences between the RVA variants can be identified. For PJ housings, frictional torques were generally larger than for SLS housings. RVAs with PU seals showed less dependency of friction on angular velocity. Figure 13 plots friction curves of AM-based RVAs with SLS housings to illustrate the effect of repeated loadings. Each data point is an average of eight individual measurements because two similar RVAs were tested in each case and both offset angles were considered.

For both sealing materials, friction changed with the number of load cycles performed. For SIL seals, friction at 0 load cycles

Figure 12 Frictional torque of AM-based RVAs as a function of angular velocity

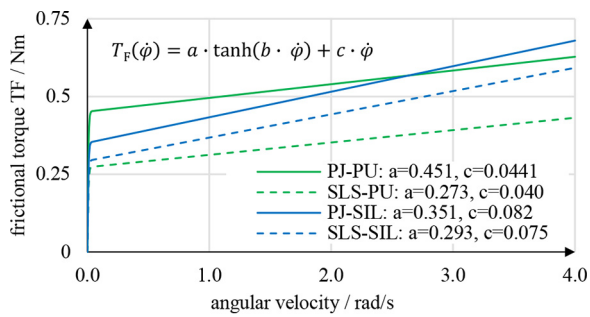

Notes: Data for calibration of the underlying friction model was obtained after 5,000–40,000 load cycles. The friction model is provided along with parameter values for AM-based RVAs with PJ (solid lines) or SLS (dashed lines) housings and PU (green lines) or SIL (blue lines) seals

Figure 13 Dependence of friction on the number of load cycles for AM-based RVAs with SLS housings and PU (solid lines) or SIL (dashed lines) seals

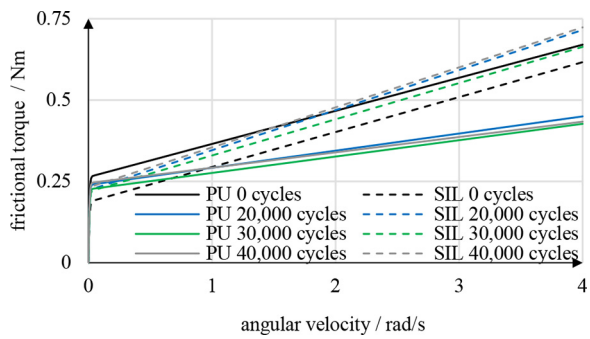

was lowest. Frictional torques at 4 rad/s increased by 16% from 0.61 Nm at 0 load cycles to 0.71 Nm at 40,000 load cycles. For PU seals, frictional torque was largest at 0 load cycles and tended to decrease with increasing number of load cycles. At 0

and 40,000 load cycles at 4 rad/s, frictional torques were 0.66 and 0.42 Nm, respectively, which equals a decrease of 36%. In fact, decreasing friction of PU RVAs and increasing friction of SIL RVAs after the initial experiment was also observed in further experiments not shown here.

4.4.3 Discussion of friction experiments

The friction behavior of the AM-based RVAs is comparable to that of the standard actuator. The absence of stick-slip behavior facilitates servo-pneumatic applications, and a friction model with suitable parameters is provided. Our results show that the friction properties of the AM-based RVAs depend on the load history and the materials used. The volatility observed may have various reasons, such as changes in the polymeric parts' stiffnesses caused by temperature changes (Bergström, 2015) and repeated loadings (Müller and Nau, 1998; Bergström, 2015), abrasion of friction surfaces and changes in the distribution of the lubricant. Because of the overall consistency of our AM-based RVAs' frictional behavior, we deem them suitable for use in functional prototyping.

4.5 Durability of additive manufacturing-based rotary vane actuators

4.5.1 Durability experiment

As shown in Figure 7, the functionality of our RVAs was investigated by repeatedly measuring leakage and friction. Between these measurements, endurance runs were performed in which the RVAs were position-controlled using the sinusoidal target profile given in equation (2). Amplitude φ_{amp} and offset position φ_{off} were set to 130° and 0°, respectively, so that the rotary vanes covered almost the entire possible range. Angular frequency was set to $\omega = 3\pi/2\,s$, and thus one load cycle was completed every $1.\overline{3}$ s. Endurance runs were performed at a mean pressure of $p_{mean} = 4$ bar.

4.5.2 Results of durability experiments

Figure 14 shows the number of load cycles completed by the AM-based RVAs, which were grouped according to material and manufacturing technology. Per group, three values are given, as each variant was manufactured twice (blue, gray) and an average value (green) is also provided. Results range from 40,000 load cycles for SLS-PU-1 up to 1,000,000 load cycles for PJ-PU-2. RVAs of type PJ-SIL, SLS-SIL and SLS-PU performed an average of 80,150; 180,000; and 145,000 load cycles, respectively. Testing of these RVAs was aborted because of excessive leakage and position error in friction testing. PJ-PU RVAs reached the highest number of load cycles, with an average of 930,000. Both experiments of this category were aborted prematurely, as no failure was foreseeable.

Figure 14 Overview of the load cycles performed in durability testing of AM-based RVAs, grouped according to the manufacturing technologies and materials used

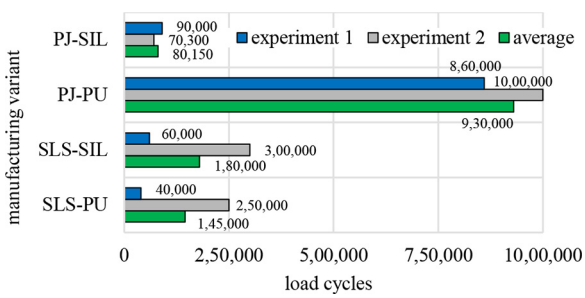

The failures can be categorized and attributed to the sealing materials used: All RVAs with SIL seals showed structural failure of the rotary vane and signs of excessive wear. As shown in Figure 15(a), sections of the circular axial seals were torn out, which resulted in inadequate sealing. Further, the surfaces of the elastomeric cylinders were considerably abraded (A), and the counter surfaces of the originally white chamber seals were clearly discolored (C). As a result of uneven wear, the rectangular elastomer parts of the chamber seals were tapered after testing (C). RVAs with PU seals showed fewer signs of wear and no structural failure of the swivels. However, in two of the PU chamber seals tested (SLS-PU-1, SLS-PU-2), the elastomer was detached from the core, as shown in Figure 15(b). Moreover, it was observed that lubrication grease leaked through the ball bearings (D) at higher load cycles, and screw heads left impressions on the PJ housings.

4.5.3 Discussion of durability experiments

Generally, functional RVAs can be manufactured using either of the materials and technologies tested. Remarkably, none of the housings showed any damage apart from minor imprints of the screw heads in the PJ housings. Seals were the cause of failure in all cases. The PU material turned out to be significantly more resistant to wear and tear. A comparison of mechanical properties, especially of tear strength, as summarized in Table 1, can largely explain this result. However, we also observed structural failure of two PU chamber seals, which we attribute to adhering powder residues from the SLS process.

Figure 15 Failure analysis of AM-based RVA parts

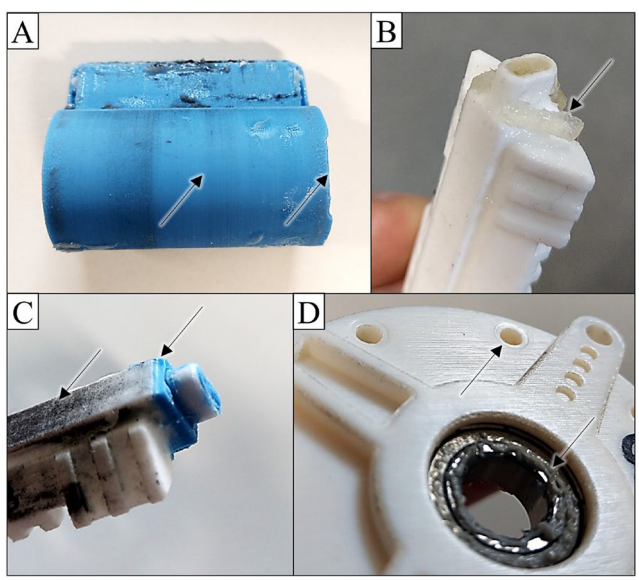

Notes: Structural failure (a and b), wear (a and c), loss off lubrication grease and deformation (d) were observed as a result of repeated loadings

5. Conclusion

We have described the replication of a commercially available pneumatic RVA by using an AM-based prototyping strategy, and have evaluated the quality of the replicas obtained in extensive component testing. Typically, RVAs have cast aluminum housings and injection-molded multi-material components that consist of hard thermoplastic cores with soft elastomeric overmolds. We redesigned the standard housings using finite element simulations and manufactured polymeric variants by PJ printing of a thermoset acrylate-based photopolymer and selective laser sintering (SLS) of a thermoplastic polyamide. Relevant surfaces were CNC milled to the final dimensions, for which we have provided machining parameters. We obtained the required multi-material components by using SLS molds to overmold SLS cores with SIL and PU elastomers and have described the exact procedure used. To evaluate the quality of the RVAs obtained, we repeatedly measured their leakage and friction properties and applied cyclic loadings between measurements. In leakage experiments performed at 6 bar differential pressure and at 0–10,000 load cycles, RVAs with SLS housings exhibited an average leakage flow of 15.2 L/min compared to 6.8 L/min for PJ housings, and RVAs with PU seals exhibited 8.0 L/min compared to 14.0 L/min for SIL seals. The combination of PU seals and PJ housings led to an average leakage flow of 0.4 L/min at 0 load cycles and increased to only 1.2 L/min at 10,000 load cycles. Thus, our RVAs can be applied for concept evaluation without further modification if low to moderate leakage is acceptable. Frictional torques of the RVAs were measured as a function of angular velocity. A suitable friction model was calibrated and has been provided. We found that, after running in, PU seals exhibited more consistent frictional properties, and we assume that increasing wear causes the more volatile behavior of the SIL components. In the endurance runs between measurements, our RVAs were position-controlled to follow a sinusoidal target profile with an amplitude of 130° and a period of $1.\overline{3}$ s. The fact that all RVAs completed at least 40,000 load cycles before excessive structural damage or leakage occurred proves the usability of the prototyping strategy applied. When manufactured properly, PU seals showed almost no signs of wear and no structural failure, which was not the case for SIL parts. The combination of PU seals and PJ housings led to an average of 930,000 load cycles, with one RVA reaching 1,000,000 load cycles without failure. With a drive torque of up to 5 Nm over an angular range of 270°, our replicas achieve the same performance as the original actuator. Because of modifications in design and the use of polymeric materials, our replicas weigh less than 226 g, which is less than 52% the weight of the original RVA (437 g). This work is of practical significance, as it enables researchers in the areas of robotics and pneumatic actuators to create prototype RVAs without the technological and economic constraints of mass production technologies. Future work will demonstrate the integration of our RVAs into a pneumatic lightweight robot.

Acknowledgment

The authors express their thanks for the opportunity to be involved in the DIMAP project, which is funded as part of the Horizon 2020 Framework program for research and innovation under grant agreement no 685937. The support received helped to initiate the work described. Most of the research was conducted at Festo SE & Co. KG (Esslingen Germany) and Johannes Kepler University Linz (Linz, Austria). Furthermore, the authors thank Luis Hermann and Felix Dangelmayr, who supported the authors in their first attempts at producing RVAs with AM technologies and in extensive component testing.

References

Baiden, D. and Ivlev, O. (2014), "Independent torque and stiffness adjustment of a pneumatic direct rotary soft-actuator for adaptable human-robot-interaction", *23rd International Conference on Robotics in Alpe-Adria-Danube Region (RAAD)*.

Belforte, G., Bertetto, A.M. and Mazza, L. (2013), "Test rig for friction force measurements in pneumatic components and seals", *Proceedings of the Institution of Mechanical Engineers, Part J: Journal of Engineering Tribology*, Vol. 227 No. 1, pp. 43-59.

Bergström, J.S. (2015), *Mechanics of Solid Polymers: Theory and Computational Modeling*, William Andrew, San Diego, CA.

Dämmer, G., Gablenz, S., Hildebrandt, A. and Major, Z. (2019), "PolyJet-printed bellows actuators: design, structural optimization and experimental investigation", *Frontiers in Robotics and Ai*, Vol. 6 No. 34.

EOS GmbH (2018), "PA 2200 performance 1.0", available at: https://eos.materialdatacenter.com/eo/material/pdf/435526/PA2200Performance1.0?sLg=de&rnd=1614869330699 (accessed March 2021).

Festo SE & Co. KG (2019), "BionicSoftArm – modular pneumatic lightweight robot", available at: www.festo.com/net/SupportPortal/Files/597075/FestoBionicSoftArm_en.pdf (accessed March 2021).

Festo SE & Co. KG (2020), "Semi – rotary drives DRVS", available at: www.festo.com/cat/de_de/data/doc_engb/PDF/EN/DRVS_EN.PDF (accessed March 2021).

Florez, J.M., Shih, B., Bai, Y. and Paik, J.K. (2014), "Soft pneumatic actuators for legged locomotion", *2014 IEEE International Conference on Robotics and Biomimetics (ROBIO)*, pp. 27-34.

Gaiser, I. Andres, A. Bretthauer, G. Breitwieser, H. Ivlev, O. Wiegand, R. and Schulz, S. (2012), "Compliant robotics and automation with flexible fluidic actuators and inflatable structures", *INTECH Open Access Publisher*.

Galloway, K.C., Becker, K.P., Phillips, B., Kirby, J., Licht, S., Tchernov, D., Wood, R.J. and Gruber, D.F. (2016), "Soft robotic grippers for biological sampling on deep reefs", *Soft Robotics*, Vol. 3 No. 1, pp. 23-33.

Galloway, K.C., Polygerinos, P., Walsh, C.J. and Wood, R.J. (2013), "Mechanically programmable bend radius for fiber-reinforced soft actuators", *2013 16th International Conference on Advanced Robotics (ICAR)*, pp. 1-6.

Gorissen, B., Reynaerts, D., Konishi, S., Yoshida, K., Kim, J.-W. and De Volder, M. (2017), "Elastic inflatable actuators for soft robotic applications", *Advanced Materials*, Vol. 29 No. 43, p. 1604977.

Grebenstein, M., Albu-Schäffer, A., Bahls, T., Chalon, M., Eiberger, O., Friedl, W., Gruber, R., Haddadin, S., Hagn, U., Haslinger, R. and Höppner, H. (2011), "The DLR hand arm system", *2011 IEEE International Conference on Robotics and Automation (ICRA)*, pp. 3175-3182.

Grzesiak, A., Becker, R. and Verl, A. (2011), "The bionic handling assistant: a success story of additive manufacturing", *Assembly Automation*, Vol. 31 No. 4, pp. 329-333.

Haddadin, S. (2013), *Towards Safe Robots: Approaching Asimov's 1st Law*, RWTH Aachen University, Aachen.

Helduser, S. and Muth, A. (1996), "Dynamic friction measurement method evaluated by means of cylinders and valves", *Fluid Power: Third JHPS International Symposium*, pp. 271-276.

Hildebrandt, A., Neumann, R. and Sawodny, O. (2009), "Optimal system design of siso-servopneumatic positioning drives", *2009 IEEE transactions on control systems technology*, pp. 35-44.

ISO/TS 15066:2017-04 (2017), *Robots and Robotic Devices – Collaborative Robots*, International Organization for Standardization, Geneva.

Kampker, A., Kreisköther, K. and Reinders, C. (2017), "Material and parameter analysis of the PolyJet process for mold making using design of experiments", *International Journal of Chemical, Molecular, Nuclear, Materials and Metallurgical Engineering*, Vol. 11 No. 3, pp. 207-214.

Kaweesa, D.V. and Meisel, N.A. (2018), "Quantifying fatigue property changes in material jetted parts due to functionally graded material interface design", *Additive Manufacturing*, Vol. 21, pp. 141-149.

Krause, J. and Bhounsule, P. (2018), "A 3D printed linear pneumatic actuator for position, force and impedance control", *Actuators*, Vol. 7 No. 2, p. 24.

Kundera, C. and Bochnia, J. (2014), "Investigating the stress relaxation of photopolymer O-ring seal models", *Rapid Prototyping Journal*, Vol. 20 No. 6, pp. 533-540.

Li, H., Yao, J., Zhou, P., Chen, X., Xu, Y. and Zhao, Y. (2020), "High-force soft pneumatic actuators based on novel casting method for robotic applications", *Sensors and Actuators A: Physical*, Vol. 306, p. 111957.

MacCurdy, R., Katzschmann, R., Youbin, K. and Rus, D. (2016), "Printable hydraulics: a method for fabricating robots by 3D co-printing solids and liquids", *2016 IEEE International Conference on Robotics and Automation (ICRA)*.

Moore, J.P. and Williams, C.B. (2015), "Fatigue properties of parts printed by PolyJet material jetting", *Rapid Prototyping Journal*, Vol. 21 No. 6, pp. 675-685.

Mosadegh, B., Polygerinos, P., Keplinger, C., Wennstedt, S., Shepherd, R.F., Gupta, U., Shim, J., Bertoldi, K., Walsh, C. J. and Whitesides, G.M. (2014), "Pneumatic networks for soft robotics that actuate rapidly", *Advanced Functional Materials*, Vol. 24 No. 15, pp. 2163-2170.

Müller, H.K. and Nau, B.S. (1998), *Fluid Sealing Technology: Principles and Applications*, Marcel Dekker, New York, NY.

Neitzert, T.R. (2015), "Accuracy of additive manufactured parts", *Key Engineering Materials*, Vol. 661, pp. 113-118.

Paydar, O.H., Paredes, C.N., Hwang, Y., Paz, J., Shah, N.B. and Candler, R.N. (2014), "Characterization of 3D-printed microfluidic chip interconnects with integrated O-rings", *Sensors and Actuators A: Physical*, Vol. 205, pp. 199-203.

Raisch, A., Mayer, A., Müller, D., Hildebrandt, A. and Sawodny, O. (2020), "A model-based cascaded control concept for the bionic motion robot", *2020 American Control Conference (ACC)*, pp. 2049-2054.

Rebong, R.E., Stewart, K.T., Utreja, A. and Ghoneima, A.A. (2018), "Accuracy of three-dimensional dental resin models created by fused deposition modeling, stereolithography, and polyjet prototype technologies: a comparative study", *The Angle Orthodontist*, Vol. 88 No. 3, pp. 363-369.

Remmers, R., Cook, D. and Gervasi, V. (2010), "Custom, integrated, pneumatic, rotary actuator for an active ankle-foot orthosis", *2010 SFF Symposium Proceedings*, pp. 816-827.

Salmoria, G.V., Leite, J.L., Vieira, L.F., Pires, A.T.N. and Roesler, C.R.M., (2012), "Mechanical properties of PA6/PA12 blend specimens prepared by selective laser sintering", *Polymer Testing*, Vol. 31 No. 3, pp. 411-416.

Schlüter, M.S. and Perondi, E.A. (2018), "Mathematical modeling of pneumatic semi-rotary actuator with friction", *Journal of the Brazilian Society of Mechanical Sciences and Engineering*, Vol. 40 No. 11, p. 523.

Schmitt, F., Piccin, O., Barb, L. and Laurent, B. (2018), "Soft robots manufacturing: a review", *Frontiers in Robotics and AI*, Vol. 5, p. 84.

Siegfarth, M., Pusch, T.P., Pfeil, A., Renaud, P. and Stallkamp, J. (2020), "Multi-material 3D printed hydraulic actuator for medical robots", *Rapid Prototyping Journal*, Vol. 26 No. 6, pp. 1019-1026.

Smooth-On, Inc. (2020), "Safety data sheet SDS no. 835", available at: www.smooth-on.com/msds/files/BD_DS_Eco_Equ_EZB_EZS_Psy_MS_OOMOO_Reb_ST_SS_Soma_Sol_Sorta.pdf (accessed March 2021).

Smooth-On, Inc. (2021), "Safety data sheet SDS no. 615", available at: www.smooth-on.com/msds/files/PMC-780.pdf (accessed March 2021).

Smooth-On, Inc. (2022a), "Smooth-Sil series, addition cure silicone rubber compounds", available at: www.smooth-on.com/tb/files/SMOOTH-SIL_SERIES_TB.pdf (accessed March 2021).

Smooth-On, Inc. (2022b), "PMC-780 dry & PMC-780 wet, industrial liquid rubber compounds", available at: www.smooth-on.com/tb/files/PMC-780_Dry-Wet.pdf (accessed March 2021).

Stratasys Ltd (2018), "PolyJet materials data sheet", available at: www.cirp.de/verfahren/Materialdaten/PolyJet-Materials-Data-Sheet.pdf (accessed March 2021).

Sun, Y., Song, Y.S. and Paik, J. (2013), "Characterization of silicone rubber based soft pneumatic actuators", *2013 IEEE/RSJ International Conference on Intelligent Robots and Systems (IROS)*, pp. 4446-4453.

Udroiu, R. and Braga, I.C. (2017), "Polyjet technology applications for rapid tooling", *MATEC Web of Conferences*, Vol. 112, p. 03011.

Vanderborght, B., Albu-Schäffer, A., Antonio, A., Burdet, E., Caldwell, D.G., Carloni, R., Catalano, M., Eiberger, O., Friedl, W., Ganesh, G. and Garabini, M. (2013), "Variable impedance actuators: a review", *Robotics and Autonomous Systems*, Vol. 61 No. 12, pp. 1601-1614.

Varga, M. and Filakovsky, F. (2020), "Design, manufacturing and problem analysis of an entirely FDM 3d printed linear pneumatic actuator", *Technical Sciences and Technologies*, Vol. 3 No. 21, pp. 98-105.

Veale, A.J. and Xie, S.Q. (2016), "Towards compliant and wearable robotic orthoses: a review of current and emerging

actuator technologies", *Medical Engineering & Physics*, Vol. 38 No. 4, pp. 317-325.

Wallin, T.J., Pikul, J. and Shepherd, R.F. (2018), "3D printing of soft robotic systems", *Nature Reviews Materials*, Vol. 3 No. 6, pp. 84-100.

Yap, Y.L., Sing, S.L. and Swee Yeong, W.Y. (2020), "A review of 3D printing processes and materials for soft robotics", *Rapid Prototyping Journal*, Vol. 26 No. 8, pp. 1345-1361.

Zhang, P. and To, A.C. (2016), "Transversely isotropic hyperelastic-viscoplastic model for glassy polymers with application to additive manufactured photopolymers", *International Journal of Plasticity*, Vol. 80, pp. 56-74.

Zinn, M., Roth, B., Khatib, O. and Salisbury, J.K. (2004), "A new actuation approach for human friendly robot design", *The International Journal of Robotics Research*, Vol. 23 Nos 4/5, pp. 379-398.

Zolfagharian, A., Kouzani, A.Z., Khoo, S.Y., Moghadam, A.A. A., Gibson, I. and Kaynak, A. (2016), "Evolution of 3D printed soft actuators", *Sensors and Actuators A: Physical*, Vol. 250, pp. 258-272.

Further reading

Festo AG & Co. KG (2017), "BionicCobot – sensitive helper for human-robot collaboration", available at: www.festo.com/net/SupportPortal/Files/462251/Festo_BionicCobot_en.pdf (accessed March 2021).

Corresponding author

Gabriel Dämmer can be contacted at: gabriel.daemmer@festo.com